

LA-UR-18-27960 (Accepted Manuscript)

Mean-force scattering potential for calculating optical properties of dense plasmas

Gill, Nathanael Matthew
Starrett, Charles Edward

Provided by the author(s) and the Los Alamos National Laboratory (2019-05-09).

To be published in: High Energy Density Physics

DOI to publisher's version: 10.1016/j.hedp.2019.02.001

Permalink to record: <http://permalink.lanl.gov/object/view?what=info:lanl-repo/lareport/LA-UR-18-27960>

Disclaimer:

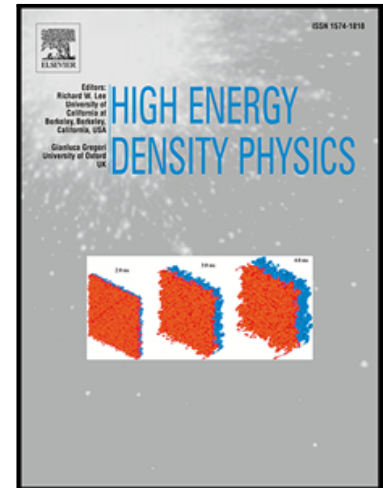
Los Alamos National Laboratory, an affirmative action/equal opportunity employer, is operated by Triad National Security, LLC for the National Nuclear Security Administration of U.S. Department of Energy under contract 89233218CNA000001. By approving this article, the publisher recognizes that the U.S. Government retains nonexclusive, royalty-free license to publish or reproduce the published form of this contribution, or to allow others to do so, for U.S. Government purposes. Los Alamos National Laboratory requests that the publisher identify this article as work performed under the auspices of the U.S. Department of Energy. Los Alamos National Laboratory strongly supports academic freedom and a researcher's right to publish; as an institution, however, the Laboratory does not endorse the viewpoint of a publication or guarantee its technical correctness.

Accepted Manuscript

Mean-Force Scattering Potential for Calculating Optical Properties of Dense Plasmas

N.M. Gill, C.E. Starrett

PII: S1574-1818(18)30071-5
DOI: <https://doi.org/10.1016/j.hedp.2019.02.001>
Reference: HEDP 668



To appear in: *High Energy Density Physics*

Received date: 23 August 2018
Revised date: 30 January 2019
Accepted date: 1 February 2019

Please cite this article as: N.M. Gill, C.E. Starrett, Mean-Force Scattering Potential for Calculating Optical Properties of Dense Plasmas, *High Energy Density Physics* (2019), doi: <https://doi.org/10.1016/j.hedp.2019.02.001>

This is a PDF file of an unedited manuscript that has been accepted for publication. As a service to our customers we are providing this early version of the manuscript. The manuscript will undergo copyediting, typesetting, and review of the resulting proof before it is published in its final form. Please note that during the production process errors may be discovered which could affect the content, and all legal disclaimers that apply to the journal pertain.

Mean-Force Scattering Potential for Calculating Optical Properties of Dense Plasmas

N.M. Gill^{a,b}, C.E. Starrett^a

^aLos Alamos National Laboratory, P.O. Box 1663, Los Alamos, NM, 87545, USA

^bAuburn University Physics Department, 206 Allison Laboratory, Auburn University, Auburn, AL 36849, USA

Abstract

We assess the relative importance of ionic structure on the opacity of dense plasmas by using the potential of mean force as a scattering potential within the Kubo-Greenwood formalism. We compare results from the potential of mean force, which includes realistic ionic structure, to results using an average atom potential, which includes only a crude treatment of ionic structure. Comparisons with less approximate but more expensive DFT-MD simulations for aluminum plasma reveal that the mean force generally improves agreement for DC conductivity. We also see improvement when applying the mean force to free-free transitions, whereas for bound-bound and bound-free transitions the mean force leads to poorer agreement on transition energies. Further, we assess the impact of accounting for correlations within the plasma at the temperature and density conditions relevant to iron opacity measurements at Sandia's Z machine facility [Bailey et al., Nature 517:56-59, 2015] and find that these correlations do not account for the discrepancy between the measurements and leading opacity calculations.

Keywords: Warm Dense Matter, Radiative Properties, Average Atom, Ion Correlations

1. Introduction

The radiative properties of dense matter are important for many active areas of research, including the solar composition problem [1, 2, 3], simulations of white dwarf stars [4], and simulations of inertial confinement fusion experiments [5, 6]. Calculating these properties, such as the electrical conductivity and the opacity, in dense systems has proven challenging. At high material densities and for temperatures below the Fermi temperature, one type of physically robust calculation involves using the Kubo-Greenwood formalism within a density functional theory molecular dynamics (DFT-MD) simulation [7, 8, 9, 10, 5, 11]. Though these calculations are considered accurate, they are computationally expensive and therefore there is need for more computationally efficient calculations applicable to a wide range of systems.

Recent experiments at the Sandia Z machine [12] have revealed a large discrepancy with state-of-the-art opacity calculations [13, 14, 15, 16], with the calculations consistently under-predicting the observed data. This has led to a search for physics that may be missing from the opacity models. One such effect that is not fully explored in modern opacity calculations is the impact of the other ions in the plasma on the electronic structure and resulting radiative properties. The optical properties of the plasma change continuously as the density of the plasma increases, meaning that effects such as continuum lowering must be modeled. Further the effects of collisions with other ions must be accounted for to fully characterize the impact of the plasma environment.

Average atom and other closely related models are computationally efficient, DFT based models that have long been used to determine various plasma properties [17, 18, 19, 20, 21, 22]. The average atom model accounts for continuum lowering self-consistently through its definition of the ion sphere and consistent treatment of bound and continuum electronic states.

Using the average atom model developed by Starrett and Saumon [23, 24], a realistic ionic structure that compares well to experiment [25] and DFT-MD simulations can be determined. It was shown by Starrett [26] that, using this average atom model as a basis, a potential of mean force could be developed that gives accurate values for the zero frequency (DC) conductivity. This potential is formed using the quantum Ornstein-Zernike equations with the electronic structure determined by the average atom calculation [23, 26] and accounts for the correlations with the surrounding electrons and ions in the plasma. Given the impact that use of the potential of mean force has on the DC conductivity, it is natural to think it may have a considerable impact on the frequency dependent AC conductivity and the opacity. In this work we assess the importance of correlations with other ions in the plasma by using this potential of mean force. We use this potential to determine the electronic states and associated matrix elements needed in the calculation of conductivity within the Kubo-Greenwood formalism.

As the calculations presented are only semi-quantitative due to the reliance on DFT and the average atom model [27], we will be looking at trends of behavior that can indicate the importance of accounting for a realistic ionic structure. We do this by comparing the results for the opacity calculated with the average atom potential to those with the potential of mean force which has the ionic structure built into it. By determining the differences in the behavior of the opacity results from the

Email addresses: ngill1@lanl.gov (N.M. Gill), starrett@lanl.gov (C.E. Starrett)

average atom and mean force approaches, we can gain insight into the effect of ionic structure on the opacity. In particular we assess the impact of those correlations for the iron plasma at conditions relevant to the Bailey et al. experiment.

This paper is organized in the following way. In Section 2 we present the main expressions that define the scattering potentials used in this work, namely the average atom potential and the potential of mean force as described in Reference [26]. From there we give the Kubo-Greenwood expression for the conductivity and describe how the opacity is determined from the conductivity. In Section 3 we first compare our results for the DC conductivity to DFT-MD simulations. Next we present the AC conductivity of our methods compared to DFT-MD. We then show that both the average atom model and mean force calculations obey the f-sum rule. Finally we present the opacity calculated with the mean force potential compared to the average atom model. We do this for several temperatures and densities of aluminum, deuterium, and iron.

2. Theory

2.1. Average Atom Potential

In our average atom calculations, the effective electronic potential is solved for self-consistently within the confines of an ion sphere whose volume is defined according to

$$n_i^0 = V_{ion}^{-1} = \left(\frac{4\pi}{3}R_{is}^3\right)^{-1} \quad (1)$$

where n_i^0 is the ion density of the plasma and R_{is} is the radius of the ion sphere [24, 17, 19], which is required to be charge neutral. The potential arising from this self-consistent calculation is given by

$$V_{eff}^{AA}(r) = -\frac{Z}{r} + \int_{V_{ion}} d\vec{r}' \frac{n_e^{AA}(r')}{|\vec{r} - \vec{r}'|} + V^{xc}[n_e^{AA}(r)] \quad (2)$$

where Z is the nuclear charge, n_e^{AA} is the electron number density coming from the average atom electronic wavefunctions, and V^{xc} is the exchange correlation potential arising from the choice of exchange-correlation functional. V_{eff}^{AA} represents the effective potential seen by the electrons within the ion sphere and is enforced to be zero for $r > R_{is}$. This has been used to calculate the opacity previously [27]. Though the model provides reasonable results, it has only a crude treatment of the surrounding ions through the definition of the ion sphere.

2.2. Potential of Mean Force

In order to more realistically account for the influence of the surrounding ions in the plasma, we use the quantum Ornstein-Zernike equations to determine a potential of mean force that is felt by the electrons. This potential accounts for the interaction of the electron with the central ion as well as ions and electrons in the surrounding plasma, and by the nature of the ionic correlations, this potential is not confined to the ion-sphere. The

expression for the resulting scattering potential is given as

$$V^{MF}(r) = V_{ie}(r) + n_i^0 \int d\vec{r}' \frac{C_{ie}(|\vec{r} - \vec{r}'|)}{-\beta} h_{ii}(r') + n_e^0 \int d\vec{r}' \frac{C_{ee}(|\vec{r} - \vec{r}'|)}{-\beta} h_{ie}(r') \quad (3)$$

where V_{ie} is the potential that includes interactions between the electron and the central nucleus and other electrons in the central ion, n_e^0 is the free electron density, C_{ie} (C_{ee}) is the electron-ion (-electron) direct correlation function from the quantum Ornstein Zernike equations, $\beta = \frac{1}{k_B T}$, and h_{ii} (h_{ie}) is the pair correlation function corresponding to the ion-ion (-electron) pair. The pair correlation function is simply related to the radial distribution function $g_x(r)$ by

$$h_x(r) = g_x(r) - 1 \quad (4)$$

Additionally, the pair correlation function can be easily used to determine the structure factor of the system

$$S_{ii}(k) = 1 + n_i^0 h_{ii}(k) \quad (5)$$

where S_{ii} is the ion-ion structure factor and $h_{ii}(k)$ is the Fourier transform of the real-space ion-ion pair correlation function, dependent on wave number k . Thus through h_{ii} the ionic structure is implicitly included in the potential of mean force. Details on the determination of V^{MF} and how it differs from V_{eff}^{AA} can be found in Ref [26].

Though all of the components used to construct V^{MF} in equation 3 are determined self-consistently, V^{MF} and the resulting electronic states are not self-consistent. This is due to the difficulty in defining a set of physical constraints within which V^{MF} can be self-consistently determined. Unlike V_{eff}^{AA} , which is determined within the confines of a charge neutral sphere of radius R_{is} , V^{MF} extends throughout all space, having a nonzero value within the volumes of other ions in the plasma. Self-consistent definitions of a potential of mean force have been developed, namely by Chihara [28]. However, such chemical models suffer from issues when applied to plasmas.

2.3. Optical Properties

The main interest of this paper is to address the effect that accounting for ion correlations through the effective electronic potential has on the optical properties of the plasma, namely the opacity and the optical conductivity. The optical conductivity $\sigma(\omega)$ can be determined from the average atom model via the Kubo-Greenwood formalism [29] by the following expression

$$\sigma_1(\omega) = \frac{1}{\omega^2 + \gamma^2} \frac{2\pi n_i^0}{\omega} \sum_{ij} (f(E_i, \mu) - f(E_j, \mu)) \times \left| \langle \psi_j | \frac{\partial V_{eff}}{\partial r} | \psi_i \rangle \right|^2 \delta(E_j - E_i - \omega) \quad (6)$$

where we have represented the matrix element in the acceleration gauge, the index $i(j)$ corresponds to the initial (final) state of the electron within the context of a photoexcitation of energy $\hbar\omega$, and γ is a renormalization constant that accounts for a finite lifetime of the scattered state. The renormalization constant is determined by forcing the following sum rule to be satisfied

$$\int_0^\infty \sigma^{ff}(\omega) d\omega = \frac{\pi e^2 \bar{n}_e^0}{2m_e} \quad (7)$$

where σ^{ff} is the part of the conductivity arising from free-free transitions and m_e is the mass of the electron [29, 30].

The conductivity is dependent on both the electronic wavefunctions and the spatial variation of the effective potential seen by the electrons. When comparing the optical conductivity as calculated by the average atom model and the mean force model, we need only determine the orbitals resulting from each potential and calculate the matrix element in Equation 6:

$$\langle \psi_j^{AA} | \frac{\partial V_{eff}^{AA}}{\partial r} | \psi_i^{AA} \rangle \rightarrow \langle \psi_j^{MF} | \frac{\partial V^{MF}}{\partial r} | \psi_i^{MF} \rangle \quad (8)$$

Equation 6 can also be formulated with explicit dependence on the ionic structure factor (see, for example, Ref [31]). When using the potential of mean force, the structure factor is implicitly present in the structure of the potential and thus does not need to be explicitly included in equation 6. In the V_{eff}^{AA} calculation with explicit $S(k)$ dependence, only the free-free profile is modified by the ionic structure of the plasma, but the implicit inclusion of ionic structure within the mean force potential means that both the continuum and bound states are affected consistently by the other ions in the plasma. Except where otherwise noted, the average atom model results presented in this work set $S(k) = 1$ so that we can gain a clearer understanding of the true importance of the plasma's ionic structure.

So far we have presented the method for determining the real part of the optical conductivity, σ_1 , but in order to determine the opacity from this calculation we also require the imaginary part of the conductivity, σ_2 . This can be obtained from the real part of the conductivity via a Kramers-Kronig relation [29, 27]. With both the real and imaginary parts of the conductivity available, we can determine the dielectric function ϵ via

$$\epsilon(\omega) = 1 + i \frac{4\pi\sigma(\omega)}{\omega} \quad (9)$$

where $\sigma = \sigma_1 + i\sigma_2$ is the complex optical conductivity. With the complex dielectric function determined, we can determine the index of refraction, $n(\omega)$ for the plasma

$$n(\omega) = \sqrt{\frac{\Re\epsilon(\omega) + |\epsilon(\omega)|}{2}} \quad (10)$$

Finally we can use the index of refraction to determine the absorption coefficient $\alpha(\omega)$ which, in media where intensity loss from scattering can be ignored such as those we are dealing with in this work, is equivalent to the opacity. The absorption coefficient is related to the real part of the optical conductivity and the index refraction according to

$$\alpha(\omega) = \frac{4\pi\sigma_1(\omega)}{n(\omega)c} \quad (11)$$

where c is the speed of light in vacuum [29, 27].

Throughout this paper, our calculations are done using the exchange-correlation functional developed by Groth et al. [32] and is labeled “qmc17” in our figures.

3. Results

3.1. DC Conductivity

Using the Kubo-Greenwood average atom and mean force formalisms as detailed in the previous section, we have calculated the optical conductivity at $\omega = 0$, i.e. the DC conductivity. We compare our results to the less approximate but costly DFT-MD calculations of Witte et al. [11] in figure 1 as a function of temperature. The V_{eff}^{AA} results generally show a significant over-prediction of the DC conductivity compared to the DFT-MD results, however there is a clear improvement in agreement as temperature increases. With explicit use of $S(k)$ in the V_{eff}^{AA} calculation, we see worse agreement than when we set $S(k) = 1$.

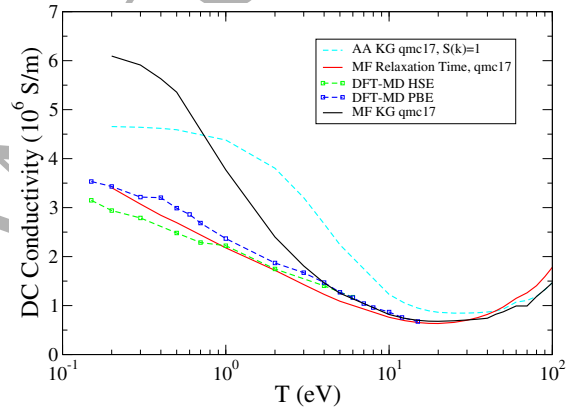


Figure 1: Here we compare the DC conductivity calculated with the average atom and mean force potentials with the results obtained by Witte et al. [11] for aluminum at solid density (2.7 g/cm^3). Witte et al. used finite-temperature DFT-MD with both the HSE and PBE functionals. We also show the results of a relaxation time approximation as is done in Ref [26] in the results labeled MF Relaxation Time.

When we compare the results of our calculation using the mean force scattering potential, we see much better agreement with the DFT-MD results for the higher temperatures. Above 3 eV the mean force calculation has excellent agreement with both the HSE and PBE DFT-MD results. The choice of exchange-correlation functional becomes less important to the DC conductivity in this regime as the two DFT-MD results become practically indistinguishable. We also see the dependence on exchange-correlation functional becoming less important at higher temperatures in our results (not shown in the figure).

For both the V_{eff}^{AA} and V^{MF} calculations, we still see large discrepancies at temperatures below 3 eV. This is possibly due to the renormalization of the Kubo-Greenwood integrals used in both models, as described in the previous section. When we use the mean force scattering potential in the relaxation time approximation as described in Reference [26], we see results that stay consistent with the DFT-MD results even at low temperatures. The relaxation time approximation does not

use explicit renormalization, but is only applied to zero frequency calculations. Given that the scattering potential is the same in our Kubo-Greenwood calculation and the relaxation time approximation, this adds credence to the argument that our Kubo-Greenwood calculations have inaccurate behavior at low temperatures due to the renormalization introduced in the formalism used. The renormalization becomes less important at higher temperatures where the assumed Drude form used in the method is more physically representative of the system.

3.2. AC Conductivity

In figure 2 we compare our calculations with DFT-MD simulations [11] for the AC conductivity of aluminum at solid density. For the low temperature case of .5 eV, the V_{eff}^{AA} and V^{MF} calculations have qualitative agreement with the DFT-MD results. At 6 eV, V^{MF} yields an AC conductivity that is significantly different from V_{eff}^{AA} , but without significantly improved agreement with the DFT-MD results. As the temperature increases to 12 eV, the mean force calculation becomes more similar to the DFT-MD results and is a marked improvement over V^{AA} at practically all frequencies.

Let us address the position of the 2p-free edge in the top inset of figure 2. Clearly the V^{MF} results are in poorer agreement with DFT-MD than the V_{eff}^{AA} results. The choice of exchange-correlation functional could cause a difference in eigenvalues which would present itself as a frequency shift in the conductivity, though we expect that the results obtained using qmc17 should be close to the DFT-MD results obtained with PBE, and the same functional is used for both the V_{eff}^{AA} and V^{MF} calculations. Ideally we would use the same functional, but it is not currently possible to use PBE in our code. The likely source of the differences in the edge position seen in figure 2 could be the lack of self-consistency between V^{MF} and the resulting electronic states. This could lead to inaccurate eigenvalues for the electronic states and thus could explain the shift in the spectra for V^{MF} that we see.

There is also a difference in how we broaden our bound states compared to the DFT-MD calculations. Specifically this leads to an apparently missing 2s to 2p bound-bound feature (near 40 eV in the DFT-MD results) in our 12 eV temperature results in figure 2. Though this transition is seen in our calculations, the method we have implemented for broadening the bound states uses the average lifetime of the free states [29] and leads to an over-broadening of the transition. With this method the transition is too weak to show up on the scale used in figure 2. In the bottom inset of figure 2 we have forced the broadening of the bound states to be such that the conductivity resulting from the 2s to 2p resonance is comparable to that of Ref [11]. With this we see that our calculations do capture the bound-bound feature.

3.3. Opacity

Deeply bound states are too tightly bound both spatially and energetically to see any significant changes due to ions in the plasma. High energy electrons see the surrounding ions as perturbative and thus show no significant changes in their electronic structure. As such the effects of ion correlations are most

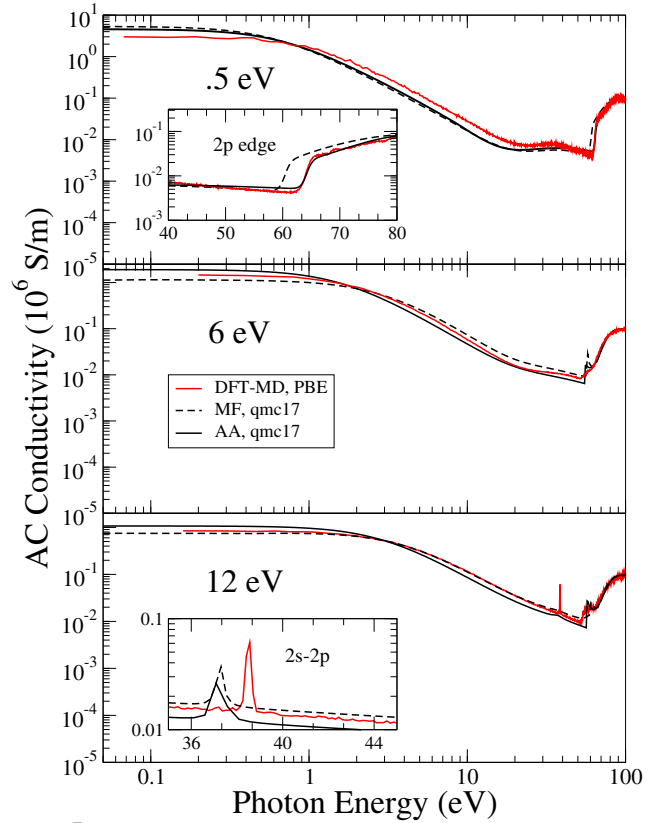


Figure 2: We compare the results of the V_{eff}^{AA} and V^{MF} calculations with the DFT-MD results of Witte et al. [11] for the AC conductivity of aluminum at solid density over several temperatures. The top inset shows the location of the 2p edge for the .5 eV case. We can see from this how the V^{MF} eigenvalues differ significantly from the DFT-MD and V_{eff}^{AA} values. The bottom inset shows the mean force results with a broadened bound state width comparable to the DFT-MD results for the 12 eV case. The difference in the frequency location of the bound-bound transition feature is due to the different exchange-correlation functionals used in the two calculations. The inset axes are the same units as the main plot.

prominently seen in loosely bound states and low energy continuum states. In figure 3 we show the opacity for aluminum at 10 eV and solid density calculated with V^{MF} , V_{eff}^{AA} , and using the V_{eff}^{AA} results for the bound-bound and bound-free transitions with the V^{MF} free-free transitions. This illustrates the relative impact of the ion correlations on the free-free transitions as compared to the bound-bound and bound-free transitions. Though use of V^{MF} changes both the continuum and bound electronic states, we can see in figure 3 that the matrix elements associated with transitions between or from bound states are less affected by ion correlations, as expected from the above physical argument.

In figure 4 we show the opacity of deuterium plasma compared to the DFT-MD results of Hu et al [5]. For all cases tested the V^{MF} calculation yields results with improved agreement to the DFT-MD calculation compared with the V_{eff}^{AA} opacity. In particular, agreement in the most non-degenerate case (5.388 g/cm³, 43.1 eV) is markedly improved, as was the case for aluminum (12 eV). The opacity shown here for deuterium arises entirely from free-free transitions in the plasma. The results in

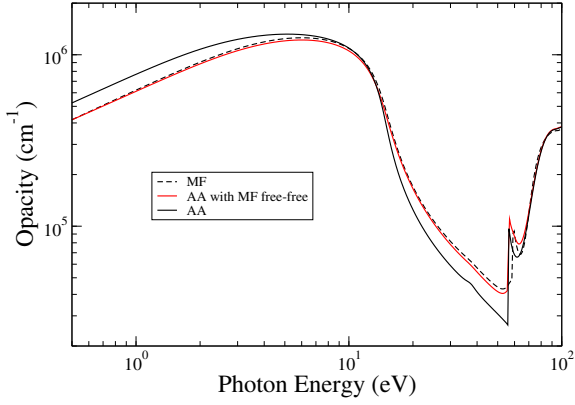


Figure 3: We compare the opacity as calculated with V_{eff}^{AA} and V^{MF} for aluminum at 10 eV and solid density. The red curve labeled “AA with MF free-free” uses the free-free part of the opacity calculated with V^{MF} and V_{eff}^{AA} bound-bound and bound-free parts of the opacity. We can see that the bound-bound and bound-free transitions are generally weakly affected by use of V^{MF} , and therefore have a small effect on the total opacity in contrast to the effect on free-free transitions.

figure 4 and the previous results for AC and DC conductivity indicate that the V^{MF} calculation generally results in more accurate results for the free-free transitions. However, for bound-bound and bound-free transitions it is not clear that V^{MF} leads to any improvement.

An important test of any opacity model is that the f-sum rule for the imaginary part of the dielectric function is satisfied [33]

$$Z = \lim_{\omega \rightarrow \infty} \frac{1}{2\pi^2 n_i^0} \int_0^\omega d\omega' \omega' \Im \epsilon(\omega') \quad (12)$$

which can also be formulated in terms of the opacity, α , and the index of refraction, n , as

$$Z = \lim_{\omega \rightarrow \infty} \frac{c}{2\pi^2 n_i^0} \int_0^\omega d\omega' n(\omega') \alpha(\omega') \quad (13)$$

In figure 5 we have shown the integral in equation 12 as a function of ω for aluminum at 1 eV and solid density. We can see that the correct number of electrons is being approached as $\omega \rightarrow \infty$ for both the V_{eff}^{AA} and V^{MF} calculations. The slight differences in the eigenvalues between the two calculations causes a small shift in the frequencies where integer number of electrons are reached, but otherwise the two calculations converge almost simultaneously to the correct number of total electrons.

3.4. Temperature and Density Effects on Ion-Correlation Features

In figure 6 we see the mass absorption coefficient (the opacity divided by the plasma mass density) for aluminum at various densities and temperatures. The influence of V^{MF} on the opacity is seen to have a complex relationship with the plasma environment. For solid density aluminum, we see very little effect at 1 eV, but the ion correlations begin to significantly change the free-free part of the opacity as the temperature is increased to 10 eV. When the temperature further increases to 20 eV, the V^{MF} results begin to approach the V_{eff}^{AA} results once again. At these

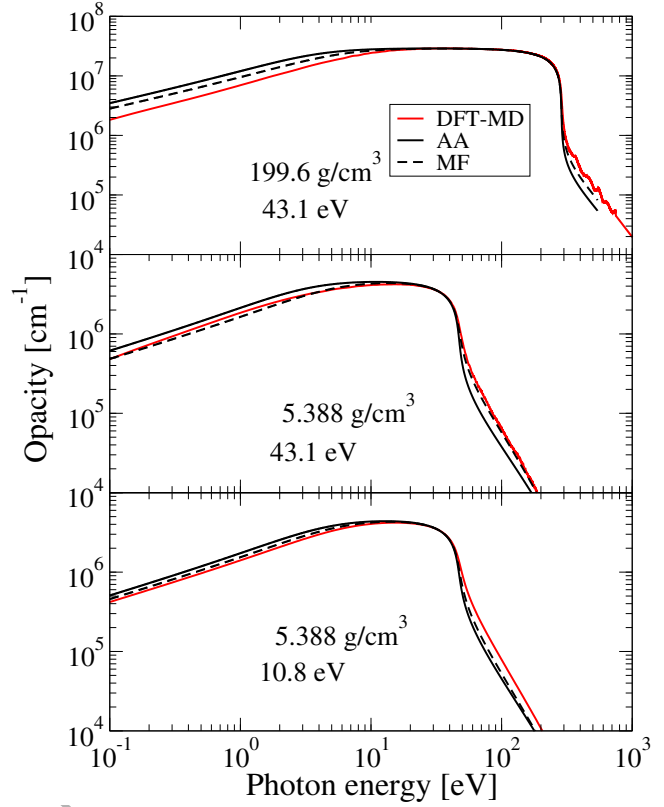


Figure 4: Opacity for deuterium at various densities and temperatures as compared to the DFT-MD results found in reference [5]. The V^{MF} results show improved agreement with the DFT-MD results compared to the V_{eff}^{AA} opacity. The opacity in this case is entirely due to free-free transitions.

higher temperatures, the electron’s thermal energy is so high that they begin to see the fields from other ions in the plasma as weak perturbations.

Figure 6 also shows how the density influences the strength of ion correlations in the plasma. Though we see little impact from V^{MF} for the 1 eV, 2.7 g/cm³ case, use of V^{MF} for the 1 eV, .027 g/cm³ case shows a more significant effect on the opacity. At the highest temperatures the influence of V^{MF} is lessened as the electrons are less coupled to the surrounding plasma. The low density cases are marked by larger spacing between the ions thus leading to weaker coupling between the electrons and surrounding ions. Hence we expect the influence of ion correlations to be weaker on the absolute opacity, though there can still be significant impact on low-lying bound states which reappear in the low density cases. It is worth noting that in figure 6, the mass absorption coefficient is shown and the low frequency features in the .027 g/cm³ case are due to the reappearing of a state that did not exist in the higher density system.

The plasma degeneracy factor, Θ , (the ratio of the thermal energy to the Fermi energy) and the plasma coupling parameter, Γ , (the ratio of the average Coulombic coupling to the thermal energy) are useful to quantify the plasma conditions where we see significant ion correlations. We show these parameters for the cases presented in figure 6, but the importance of the ion

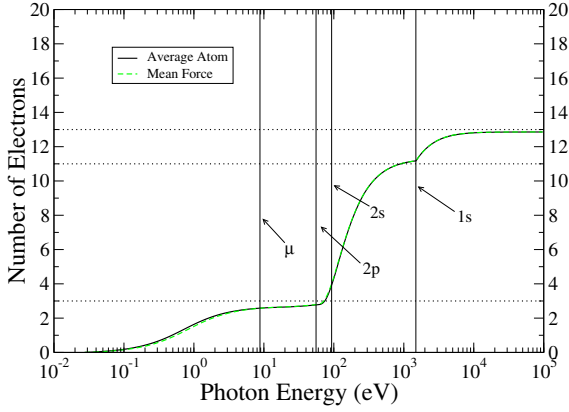


Figure 5: We show the f-sum rule for the opacity as a function of frequency for aluminum at 1 eV and solid density. The high frequency limit is the total number of electrons. The eigenvalues of the average atom electronic states are shown, as well as the chemical potential, μ , of the system, which is the same in both the V_{eff}^{AA} and V_{eff}^{MF} calculation.

correlations do not follow any discernible trend among the degeneracy and plasma coupling parameters. These parameters do not sufficiently characterize the system as to indicate when ionic correlations at the level we account for them will be of relevance for optical properties.

In figure 7 we show the mass absorption coefficient for iron at various temperatures and densities. By looking at the solid density (7.874 g/cm^3), 3 eV and 10 eV cases, we can see that the V_{eff}^{AA} and V_{eff}^{MF} results are vastly different. The results of Fu et al. [34] show that the DC conductivity for iron from 10^4 K to $3 \times 10^4 \text{ K}$ should be around $2 \times 10^6 \text{ S/m}$, and the experimental measurements of Powell give the conductivity of liquid iron at the melting point to be approximately $.719 \times 10^6 \text{ S/m}$ [35]. Our V_{eff}^{MF} results for iron at 3 eV are $5.30 \times 10^6 \text{ S/m}$ whereas the V_{eff}^{AA} results are $.046 \times 10^6 \text{ S/m}$, indicating that the V_{eff}^{MF} calculations are more accurate than the V_{eff}^{AA} results in these lower temperature, solid density cases. The under-predictive behavior of the V_{eff}^{AA} results is also in line with similar results obtained for tungsten and gold by Ovechkin et al [21] at low temperatures, where it was explained as being due to not including ion correlations in their calculations, a conclusion supported by our results.

Finally we present the results of our calculation for iron at 182 eV and $.4 \text{ g/cm}^3$ in figure 8. This case was chosen because it corresponds to the conditions thought to describe the experiment at Sandia's Z machine, which shows a dramatic difference with current state-of-the-art opacity calculations [12]. We do not see any significant difference between the V_{eff}^{MF} and V_{eff}^{AA} calculations for this density and temperature and certainly no differences that could account for any of the discrepancies between the experiment and current high-fidelity opacity calculations. A comparison of the V_{eff}^{AA} and V_{eff}^{MF} opacities at the wavelength range of the Bailey et al. experiment is shown in figure 9. This qualitatively corresponds to similar findings using a different model for the ion-correlations found by Krief et al. [36]. It is worth pointing out however, that the effect of multiple scattering (i.e. a multi-center calculation) is not included here, in either the average atom or potential of mean force ap-

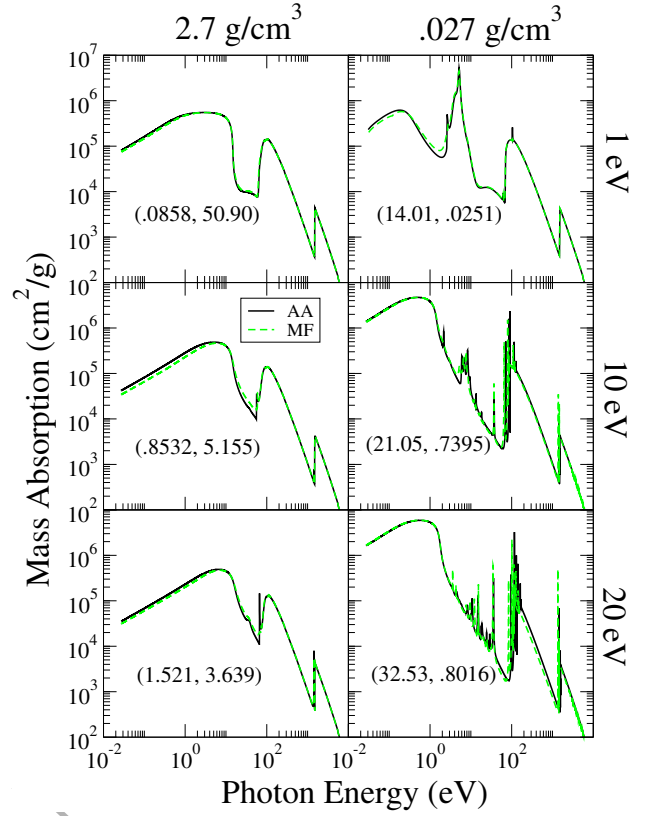


Figure 6: Mass absorption coefficient for various densities and temperatures of aluminum, which is the opacity divided by the mass density of the plasma. The V_{eff}^{AA} results are in black with the V_{eff}^{MF} results in dashed green. The values of the electron degeneracy parameter, Θ , and the plasma coupling parameter, Γ , are shown as (Θ, Γ) for each temperature and density.

proaches. To our knowledge, such a calculation is not possible with current techniques.

Though our findings qualitatively agree with Krief et al. for iron in the energy range of the Sandia experiment, they see a distinct difference in opacity between their ion sphere and ion correlation models at lower frequencies. The ion correlation model used in Reference [36] was developed by Rozsnyai [37] and involves a self-consistent calculation in which there is a significant change to the system chemical potential as compared to an average atom calculation. In contrast, our mean force calculation preserves the chemical potential and hence the state occupations of the underlying average atom calculation but uses the mean force scattering potential in the matrix elements used to determine the optical properties of the plasma. Since our calculation also preserves the ionization determined by the average atom model, it is not surprising that we see significant differences in our calculation versus that of Reference [36], especially in the free-free and bound-free transitions corresponding to the loosely bound states.

4. Conclusion

We have presented the calculation of plasma conductivity and opacity in the Kubo-Greenwood formalism with the ef-

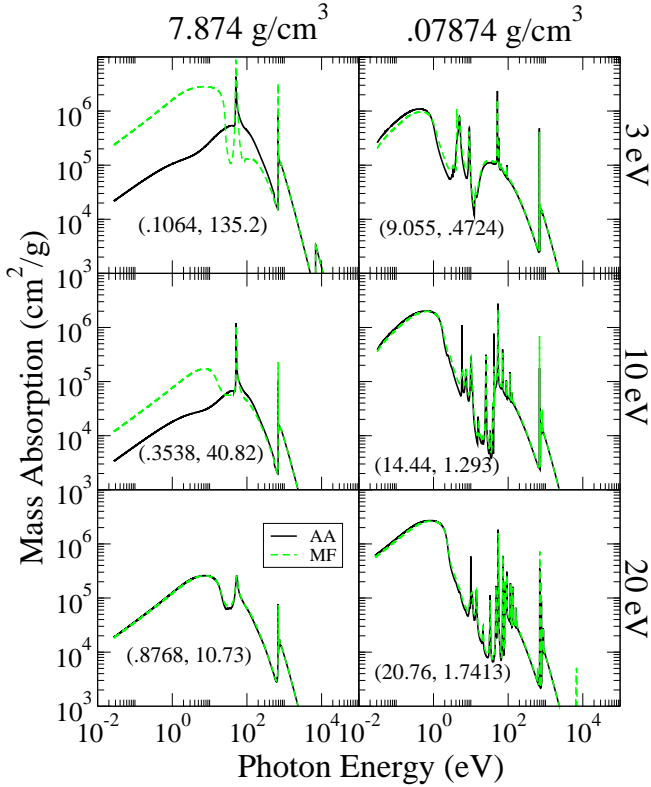


Figure 7: Mass absorption coefficient for various densities and temperatures of iron. The V_{eff}^{AA} results are in black with the V_{eff}^{MF} results in dashed green. The values of the electron degeneracy parameter, Θ , and the plasma coupling parameter, Γ , are shown as (Θ, Γ) for each temperature and density. The low temperature, solid density results show that the average atom calculation has difficulties fully capturing the free-free opacity.

fects of ion-correlations accounted for using the model developed by Starrett [26]. We see that ion-correlations can have a significant impact on the free-free transitions that dominate the DC conductivity and the opacity at low frequencies. Our V_{eff}^{MF} DC conductivity calculations show improved agreement with high-fidelity DFT-MD calculations [11] of aluminum for most plasma conditions as compared to calculations using the V_{eff}^{AA} scattering potential in the Kubo-Greenwood matrix elements. The results for the AC conductivity are less clear, but V_{eff}^{MF} generally shows greater agreement with DFT-MD simulations compared to V_{eff}^{AA} .

The results for the deuterium plasma show that the opacity has improved agreement with DFT-MD calculations through the use of V_{eff}^{MF} over V_{eff}^{AA} . The opacity in this plasma is purely due to free-free transitions. Given the improvements seen using V_{eff}^{MF} to calculate the DC conductivity, which is also caused by free-free transitions, the data show that use of V_{eff}^{MF} generally results in a more accurate representation of optical properties in systems where free-free transitions dominate. However, no obvious improvement is observed for bound-bound and bound-free transitions. This is likely due to the fact that the V_{eff}^{MF} states are not determined self-consistently, which would lead to shifts in the bound-bound and bound-free transition frequencies. A self-consistent determination of V_{eff}^{MF} and its associated elec-

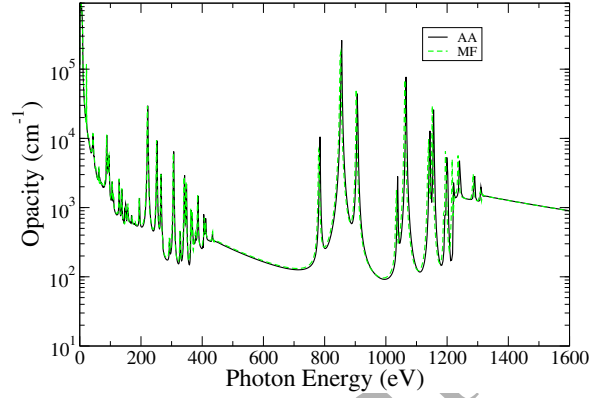


Figure 8: We show the calculation of the iron opacity at 182 eV and $.4 \text{ g/cm}^3$. The differences between the V_{eff}^{AA} and V_{eff}^{MF} calculations are small, and only has appreciable difference in the 400 eV to 800 eV range, though we see far less of a significant difference in this frequency range when compared to Krieff et al [36].

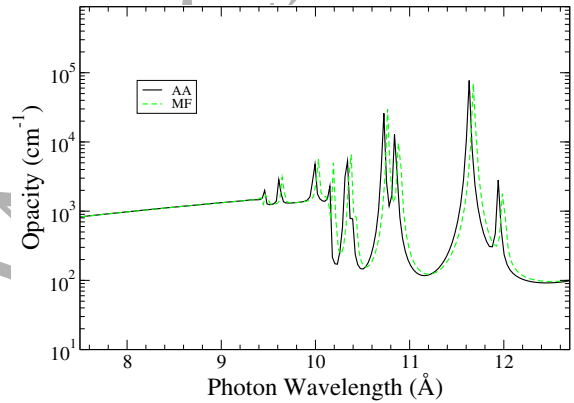


Figure 9: We show the calculation of the iron opacity at 182 eV and $.4 \text{ g/cm}^3$ in the range accessible by the Bailey et al. experiment [12]. The differences we see between the two calculations are negligible compared to the discrepancies highlighted by the experiment, indicating that the effect of ion correlations does not account for the missing opacity. Since the average atom model cannot resolve individual ion stages, there is no meaning in directly comparing to the experimental data.

tronic structure would require a new model and is beyond the scope of this work. In Shaffer et al.'s [27] determination of the free-free opacity, two different model potentials were required to determine the opacity in deuterium and aluminum, the pseudoatom and average atom potentials, respectively. Our work shows that we can obtain reasonable results for the free-free opacity through use of V_{eff}^{MF} regardless of the system under study.

For the temperatures and densities where ion correlations are significant, we see that using V_{eff}^{MF} to determine the opacity has a significant impact on the free-free profile, while it has a weak effect on the bound-free and bound-bound profiles. The V_{eff}^{MF} and V_{eff}^{AA} calculations are both shown to give reasonable results and satisfy the f-sum rule for the cases tested.

The relative importance of the ion-correlations is shown to depend on the plasma environment, with the effect generally becoming smaller in low density or high temperature plasmas. When assessing the relative importance of the correlations for

iron at the conditions measured by Bailey et. al [12], we see no appreciable difference between the standard average atom calculation and the mean force calculation. This indicates that ion-correlations, accounted for at the level of our current model, cannot explain the discrepancy between the experimental measurements and modern opacity calculations.

Acknowledgments

We would like to thank B. B. L. Witte for providing us the DFT-MD data. This work was performed under the auspices of the United States Department of Energy under contract DE-AC52-06NA25396.

- [1] A. M. Serenelli, S. Basu, J. W. Ferguson, and M. Asplund. New solar composition: the problem with solar models revisited. *Astrophys. J.*, 705:L123–L127, 2009.
- [2] M. Asplund, N. Grevesse, J. A. Sauval, and P. Scott. The chemical composition of the sun. *Annu. Rev. Astron. Astrophys.*, 47:481–522, 2009.
- [3] E. Caffau, H.-G. Ludwig, M. Steffen, B. Freytag, and P. Bonifacio. Solar chemical abundances determined with a co5bold 3d model atmosphere. *Sol. Phys.*, 268:255–269, 2011.
- [4] R. Piron and T. Blenski. Average-atom model calculations of dense-plasma opacities: Review and potential applications to white-dwarf stars. *Contrib. Plasma Phys.*, 58:30–41, 2018.
- [5] S. X. Hu, L. A. Collins, T. R. Boehly, J. D. Kress, V. N. Goncharov, and S. Skupsky. First-principles thermal conductivity of warm-dense deuterium plasmas for inertial confinement fusion applications. *Phys. Rev. E*, 89:165113, 2014.
- [6] S. X. Hu, V. N. Goncharov, T. R. Boehly, R. L. McCrory, S. Skupsky, L. A. Collins, J. D. Kress, and B. Militzer. Impact of first-principles properties of deuterium-tritium on inertial confinement fusion target designs. *Physics of Plasmas*, 22:056304, 2015.
- [7] R. Kubo. Statistical-mechanical theory of irreversible processes. i. general theory and simple applications to magnetic and conduction problems. *J. Phys. Soc. (Japan)*, 12:570–586, 1957.
- [8] D. A. Greenwood. The boltzmann equation in the theory of electrical conduction in metals. *Proc. Phys. Soc. (London)*, 71:585, 1958.
- [9] M. P. Desjarlais, J. D. Kress, and L. A. Collins. Electrical conductivity for warm, dense aluminum plasmas and liquids. *Phys. Rev. E*, 66:025401(R), 2002.
- [10] B. Holst, M. French, and R. Redmer. Electronic transport coefficients from ab initio simulations and applications to dense liquid hydrogen. *Phys. Rev. B*, 83:235120, 2011.
- [11] B. B. L. Witte, P. Sperling, M. French, V. Recoules, S. H. Glenzer, and R. Redmer. Observations of non-linear plasmon damping in dense plasmas. *Physics of Plasmas*, 25:056901, 2018.
- [12] J. E. Bailey, T. Nagayama, G. P. Loisel, G. A. Rochau, C. Blancard, J. Colgan, Ph. Cosse, G. Faussurier, C. J. Fontes, F. Gilleron, I. Golovkin, S. B. Hansen, C. A. Iglesias, D. P. Kilcrease, J. J. MacFarlane, R. C. Mancini, S. N. Nahar, C. Orban, J.-C. Pain, A. K. Pradhan, M. Sherril, and B. G. Wilson. A higher-than-predicted measurement of iron opacity at solar interior temperatures. *Nature*, 517:56–59, 2015.
- [13] J. Colgan, D. P. Kilcrease, N. H. Magee, M. E. Sherrill, J. Abdallah Jr., P. Hakel, C. J. Fontes, J. A. Guzik, and K. A. Mussack. A new generation of los alamos opacity tables. *Astrophys. J.*, 817:116, 2016.
- [14] S. Hansen, J. Bauche, C. Bauche-Arnoult, and M. Gu. Hybrid atomic models for spectroscopic plasma diagnostics. *High Energy Density Phys.*, 3:109–114, 2007.
- [15] C. A. Iglesias and F. J. Rogers. Opacities for the solar radiative interior. *Astrophys. J.*, 371:408–417, 1991.
- [16] Q. Porcherot, J.-C. Pain, F. Gilleron, and T. A. Blenski. A consistent approach for mixed detailed and statistical calculation of opacities in hot plasmas. *High Energy Density Phys.*, 7:234–239, 2011.
- [17] David A. Liberman. Self-consistent field model for condensed matter. *Phys. Rev. B*, 20:4981–4989, Dec 1979.
- [18] R. Piron and T. Blenski. Variational-average-atom-in-quantum-plasmas (vaaqp) code and virial theorem: Equation-of-state and shock-hugoniot calculations for warm dense al, fe, cu, and pb. *Phys. Rev. E*, 83:026403, Feb 2011.
- [19] B. Wilson, V. Sonnad, P. Sterne, and W. Isaacs. Purgatorio—a new implementation of the inferno algorithm. *J. Quant. Spect. Rad. Trans.*, 99:658, 2006.
- [20] G. Faussurier, C. Blancard, P. Renaudin, and P.L. Silvestrelli. Electrical conductivity of warm expanded al. *Phys. Rev. B*, 73:075106, 2006.
- [21] A. A. Ovechkin, P. A. Loboda, and A. L. Falkov. Transport and dielectric properties of dense ionized matter from the average-atom reseoos model. *High Energy Density Phys.*, 20:38–54, 2016.
- [22] M. W. C. Dharma-wardana, D. D. Klug, L. Harbour, and L. J. Lewis. Isochoric, isobaric, and ultrafast conductivities of aluminum, lithium, and carbon in the warm dense matter regime. *Phys. Rev. E*, 96:053206, 2017.
- [23] C. E. Starrett and D. Saumon. Electronic and ionic structures of warm and hot dense matter. *Phys. Rev. E*, 87:013104, Jan 2013.
- [24] C.E. Starrett and D. Saumon. A simple method for determining the ionic structure of warm dense matter. *High Energy Density Physics*, 10(0):35–42, 2014.
- [25] C. E. Starrett and D. Saumon. Models of the elastic x-ray scattering feature for warm dense matter aluminum. *Phys. Rev. E*, 92:033101, 2015.
- [26] C. E. Starrett. Potential of mean force for electrical conductivity of dense plasmas. *High Energy Density Phys.*, 25:8–14, 2017.
- [27] N. R. Shaffer, N. G. Ferris, J. Colgan, D. P. Kilcrease, and C. E. Starrett. Free-free opacity in dense plasmas with an average atom model. *High Energy Density Phys.*, 23:31–37, 2017.
- [28] J. Chihara. Unified description of metallic and neutral liquids and plasmas. *J. Phys. Condens. Matter*, 3:8715, 1991.
- [29] W. R. Johnson, C. Guet, and G. F. Bertsch. Optical properties of plasmas based on an average-atom model. *J. Quant. Spect. Rad. Trans.*, 99:327, 2006.
- [30] M. Yu. Kuchiev and W. R. Johnson. *Phys. Rev. E*, 78:026401, 2008.
- [31] C. E. Starrett. Kubo-greenwood approach to conductivity in dense plasmas with average atom models. *High Energy Density Phys.*, 19:58–64, 2016.
- [32] S. Groth, T. Dornheim, T. Sjostrom, F. D. Malone, W. M. C. Foulkes, and M. Bonitz. Ab initio exchange-correlation free energy of the uniform electron gas at warm dense matter conditions. *Phys. Rev. Lett.*, 119:135001, 2017.
- [33] M. P. Prange, J. J. Rehr, G. Rivas, J. J. Kas, and John W. Lawson. Real space calculation of optical constants from optical to x-ray frequencies. *Phys. Rev. B*, 80:155110, 2009.
- [34] Z. J. Fu, Q. F. Chen, X. R. Chen, X. W. Sun, and W. L. Quan. Electrical conductivity and nonmetal-metal transition of dense iron and nickel plasmas. *Phys. Scr.*, 85:045502, 2012.
- [35] R. W. Powell. The electrical resistivity of liquid iron. *The London, Edinburgh, and Dublin Philosophical Magazine and Journal of Science*, 354:772–775, 1953.
- [36] M. Krief, Y. Kurzweil, A. Feigel, and D. Gazit. The effect of ionic correlations on radiative properties in the solar interior and terrestrial experiments. *The Astrophysical Journal*, 856:2, 2018.
- [37] B. F. Rozsnyai. Photoabsorption in hot plasmas based on the ion-sphere and ion-correlation models. *Phys. Rev. A*, 43:3035, 1991.